Journal of Science and Technology in Civil Engineering, NUCE 2021. 15 (1): 90–101

MICROSTRUCTURAL CHARACTERISTICS OF ULTRA-HIGH PERFORMANCE CONCRETE BY GRID NANOINDENTATION AND STATISTICAL ANALYSIS

Pham Thai Hoan[a,*], Ngo Tri Thuong[b]

[a]*Faculty of Building and Industrial Construction, National University of Civil Engineering, 55 Giai Phong road, Hai Ba Trung district, Hanoi, Vietnam*
[b]*Faculty of Civil Engineering, Thuyloi University, 175 Tay Son street, Dong Da district, Hanoi, Vietnam*

Article history:
Received 25/08/2020, Revised 12/12/2020, Accepted 14/12/2020

Abstract

In this study, grid nanoindentation and statistical deconvolution analysis were applied into a developed Ultra-high performance concrete (UHPC) to broaden the understanding of the microstructure phases and their mechanical properties. A total of 550 nanoindentation tests was carried out on UHPC and the mechanical properties, including indentation modulus and hardness of the indented material were extracted from nanoindentation load-depth curves. The statistical deconvolution analysis was then utilized to analyze the modulus and hardness spectra. The experimental and analysis results revealed that the modulus and hardness data obtained from nanoindentation tests can be used in the accurate and reliable identification of the microstructure phases and their properties in UHPC. For the present UHPC, the microstructure can be characterized into 6 phases with distinguishable mechanical properties, including micro porosity, Low Density Calcium Silicate Hydrates (LD CSH), High Density Calcium Silicate Hydrates (HD CSH), silica powder and sand, and residual cement clinker. The obtained modulus and hardness values of these phases were in the range of various reported ones for cement-based materials and UHPC.

Keywords: ultra-high performance concrete; microstructures; micromechanical properties; nanoindentation; statistical analysis.

https://doi.org/10.31814/stce.nuce2021-15(1)-08

1. Introduction

Ultra-high performance concrete (UHPC), a new generation of concrete, has been developed and become a widely used material in industrial and structural applications [1, 2]. Several researchers have investigated and manufactured concretes that could be classified as UHPC, leading to the development of various types of UHPC. Nevertheless, UHPC can be generally characterized by a very high compressive strength of greater than 150 MPa [3]. This type of material exhibits predominant mechanical properties over the previous classes of concrete such as high flowability, advanced strength, long-term stability, and excellent durability [4]. The superior performance of UHPC is gorverned by their microstructures, which is tailored by increasing the packing density with a low water-to binder ratio ($w/b < 0.25$) and high binder contents, including special aggregates such as silica fume, quartz

*Corresponding author. *E-mail address:* hoanpt@nuce.edu.vn (Hoan, P. T.)

powder, adequate sand gradation, and super plasticizer (high-range water reducer) [5]. Thus, the comprehensive understanding of microstructures and their properties, which are determinant of UHPC performance, is essential for the development of UHPC. To explore the knowledge of UHPC microstructure and its properties, besides the qualitative methods such as image analyses, the quantitative approaches have been commonly utilized. The advanced instrumentation techniques with high spatial resolution that allow characterizing the mechanical properties of a material and its microstructure phases at micro and nano scales have been considered the preferred methods among the quantitative approaches [6, 7]. One such instrumentation technique is nanoindentation, which is now becoming an effective and widely used tool for evaluation of the material local properties at small scales such as micro or nano levels.

The basic principle of nanoindentation technique is to indent a hard tip that is normally made of diamond into a material surface and the material properties then can be extracted from the response under the tip [8, 9]. It has shown high efficiency in determining mechanical properties of various material types by providing reliable results on ceramics, steel, glass, bone, and especially cementitious materials such as geopolymer paste or UHPC [6, 9–12]. Indeed, a recent review study has reported that valuable knowledge of the microstructural phases and their mechanical properties of cementitious materials such as cement pastes blended with meta-kaolin, silica fume, nanosilica, cement pastes and cement clinkers with various cement-water ratios, and also of different alkali-activator as slag and fly ash, and UHPC were gained by using nanoindentation combining with statistical deconvolution analysis [6]. These successful investigations motivated the application of the combined nanoindentation and statistical analysis into a developed UHPC material in this study.

The aim of present work is to broaden the understanding of the microstructure phases and their mechanical properties of the proposed UHPC material using grid nanoindentation and statistical deconvolution analysis. The achieved results shall provide the important knowledge that are helpful to produce UHPC with better performance.

2. Methods

2.1. Nanoindentation technique

It is briefly recalled that a nanoindentation test consists of establishing contact between an indenter (typically diamond) and a sample, and subsequently measuring the load P and the penetration depth h [13]. Fig. 1 illustates a typical nanoindentation $P-h$ curve, which provides the information related to the correlation between the indenter and indented materials.

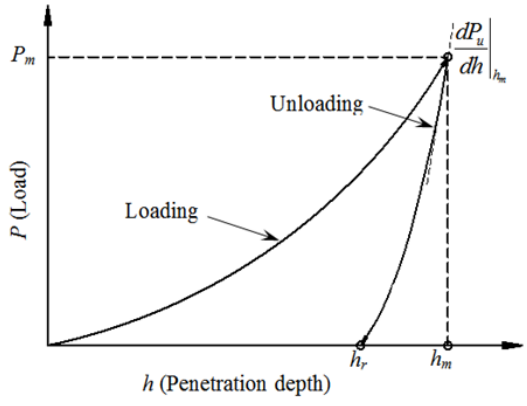

Figure 1. Typical $P-h$ curve

By analyzing the $P-h$ curve, the indentation modulus M and indentation hardness H of the indented material can be derived as follows [11, 14–17]:

$$M = \frac{\sqrt{\pi}}{2\beta}\frac{S}{\sqrt{A_c}} \text{ and } H = \frac{P_m}{A_c} \qquad (1)$$

where $S = dP_u/dh|_{h_m} = mB(h_m - h_r)^{m-1}$ with $B(h_m - h_r)^m$ is the fitting power-law function of the unloading portion P_u of $P-h$ curve; β is the factor related to indenter shape; $A_c = 24.5h_c^2$ is the

projected contact area where contact depth $h_c = h_m - \varepsilon^* P_m/S$ and $\varepsilon^* = 0.75$ for sharp indenters; P_m, h_m, and h_r is the maximum load, the maximum depth, and the residual depth, respectively, that can be directly measured from the $P - h$ curve. The indentation modulus M is considered the reduced modulus owing to the effects of elastic deformation of the indenter, and can be linked to the elastic modulus E of the isotropic indented material following the relation [14]:

$$M = \left(\frac{1 - \upsilon^2}{E} + \frac{1 - \upsilon_i^2}{E_i} \right)^{-1} \tag{2}$$

where E, υ, and E_i, υ_i are the elastic modulus and Poisson's ratio of the material and indenter, respectively.

2.2. *Statistical deconvolution analysis*

Statistical deconvolution analysis based on the nanoindentation results has been proved to be a powerful tool for examining the microstructure phases and their properties of cementitious composite materials, including UHPC [6, 10, 18]. The principles of this combining approach are: (i) the large indentation depth leads to the assessment of homogenized material properties, whereas the small nanoindentation depth leads to the assessment of microstructural phase properties, which are given by Gadanken experiment [19]; (ii) a large enough number of small nanoindentation depths could lead to the identification and quantification of microstructure phases from the distinguishable material properties using statistical deconvolution analysis, as illustrated in Fig. 2, where PDF denotes for Probability Density Function.

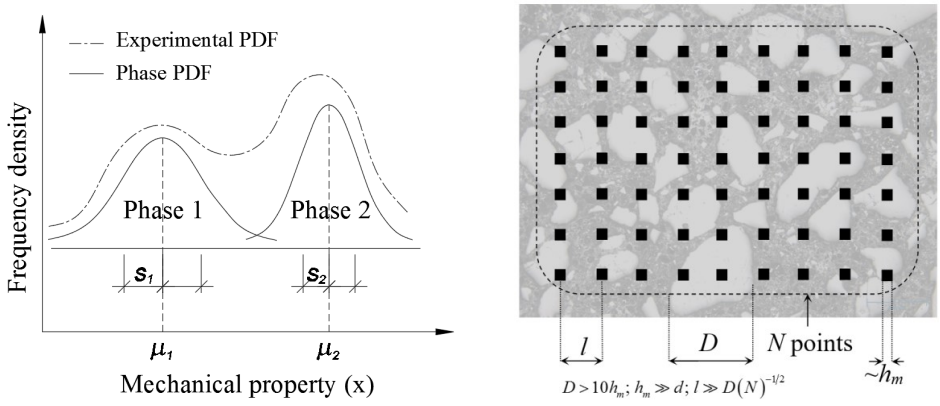

Figure 2. Principle of statistical deconvolution analysis for composite materials

Typically, a large number of nanoindentation need to be carried out on an area of the sample surface for the identification of the phases. For example, 100 indentations are sufficient to guarantee a convergence on the elastic property of two intrinsic properties of two characteristic morphological arrangements of Calcium Silicate Hydrates (CSH) in cement based materials, namely the High Density CSH (HD CSH) and the Low Density CSH (LD CSH) with an error less than 5% [5, 20]. Once the test number N is sufficient, the volume fraction (i.e. volume/surface fraction f_J) of a mechanically distinguishable microstructural phase (J) can be expressed as:

$$f_J = N_J/N \tag{3}$$

where N_J is the nanoindentation test number on the phase J. The volume fraction of or the test number on the phases obeys the constraint:

$$\sum_{J=1}^{n} f_J = 1 \text{or} \sum_{J=1}^{n} N_J = N \tag{4}$$

where n is the number of mechanically distinguishable material phases. The statistical analysis allows to determine the volume fraction, mean value (μ_J), and standard derivation (s_J) of the material phases from mechanical property $x = (M, H)$ of each phase J based on the principle of deconvolution analysis technique that the property $x = (M, H)$ of phase J is best approximately described by a normal or Gaussian function [21]:

$$\psi_J(x) = \frac{1}{s_J\sqrt{2\pi}} \exp\left(\frac{-(x-\mu_J)^2}{2s_J^2}\right) \tag{5}$$

where

$$\mu_J = \frac{1}{N_J}\sum_{k=1}^{N_J} x_k \text{ and } s_J^2 = \frac{1}{N_J - 1}\sum_{k=1}^{N_J}(x_k - \mu_J) \tag{6}$$

The theoretical probability density function (PDF) of all property values obtained from nanoindentation tests called convolution function is then expressed as:

$$PDF = \sum_{J=1}^{n} f_J \psi_J(x) \tag{7}$$

All the unknown parameters μ_J, s_J, and f_J of each constitutive phase then can be determined from the PDF that most suitably describes the experimental PDF (PDF_{exp}) obtained from nanoindentation data. The best suitable description (so called best-estimated PDF or theoretical PDF) of the test data is found from the minimum standard error between the theoretical and experimental PDFs, as follows:

$$\text{Find } (\mu_J, s_J, f_J) \text{ from } \min \sum_{i=1}^{m} \frac{[PDF_{\text{exp}}(x_i) - PDF(x_i)]^2}{m} \tag{8}$$

where m is the number of the bins (intervals), which are appropriately chosen in the construction of the experimental PDF.

In addition, to identify statistically revelant phase properties with a sufficient contrast, the overlap of successive normal distributions representative of two phases is constrained by [5]:

$$\mu_J^x + s_J^x < \mu_{J+1}^x + s_{J+1}^x \text{ where } x = (M, H) \tag{9}$$

The combined nanoindentation tests and statistical deconvolution analysis described above are used to investigate the microstructure phases and their properties of a proposed UHPC in this study.

3. Experiments

3.1. Material and specimen preparation

A proposed type of UHPC with the composition in weight ratio and mean particle size listed in Table 1 is used in this study. The UHPC mixture was mixed by a Hobart type laboratory mixer. Silica

sand and Silica fume were first dry-mixed for 5 min before silica powder and cement were added and further mixed in 5 min. The water and superplasticizer then were gradually poured into the mixture and continuously mixed until the paste shown adequate workability. The flowability of the mixture was checked by a flow test [22]. The mixture was poured into plastic molds without vibration to form the specimen shape. All specimens were stored in a laboratory at room temperature for 48h prior to demolding. The specimens were then cured at 90 ± 3 °C for 72h in a hot water tank. After curing, the specimens were stored in dry condition for at least 28 days. The compressive strength of UHPC was obtained to be 184 MPa from the test results on five cubic specimens ($50 \times 50 \times 50$ mm^3). For nanoindentation sample, the UHPC specimens were first sliced into three penny shaped samples of 20 mm in diameter with a thickness of 10 mm, named S1, S2, and S3. The samples were then mounted in epoxy and polished in seven stages by silicon carbide papers, poly diamond particles, and colloidal silica with the fineness of the last stage about 40 nm to obtain a flat and smooth surface. This polishing procedure, which conforms to ASTM E3-01 standard [23], was carefully undertaken to eliminate the surface roughness in the similarity analysis and minimize any errors occurred during nanoindentation tests [24].

Table 1. Composition and particle size of UHPC compounds

	Cement type I	Silica sand	Silica fume	Silica powder	Super-plasticizer	Water
Composition (in *wt*. ratio)	1	1.1	0.25	0.30	0.067	0.2
Mean particle size (μm)	10-25	50-300	0.1-1	1-50	-	-

3.2. Nanoindentation test

Nano Hardness Tester equipped with a Berkovich indenter was used for nanoindentation tests, which were carried out at room temperature according to ASTM E2546-07 standard [25]. The indenter made of diamond has an elastic modulus of $E_i = 1141$ GPa and Poisson's ratio of $\upsilon = 0.07$. Fig. 3 presents the polished nanoindentation sample and the installation of the sample in the testing machine.

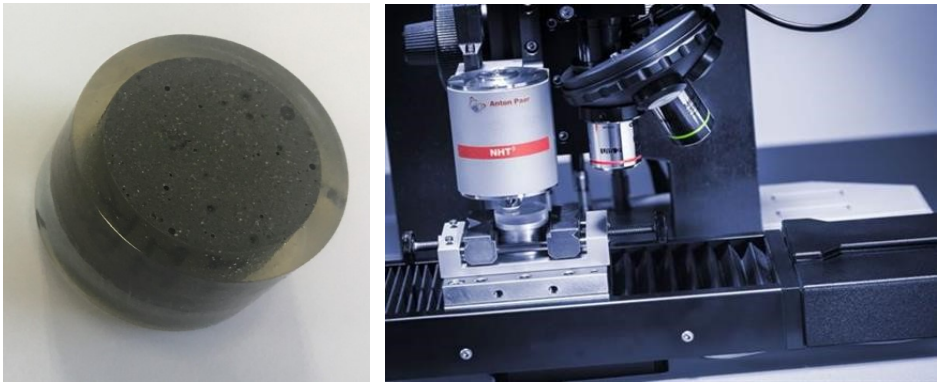

Figure 3. Polished nanoindentation sample and its installation in testing machine

A total of 550 indenting points consisting five lines of 110 nanoindentataion tests with the spacing of 10 μm was performed with maximum load of 2 mN under a rate of 4 mN/min for both loading and unloading. It is noted that among five indenting lines, three lines were performed on sample

S1 and one indenting line on the remaining samples, S2 and S3. The above test number, spacing of indents, and the maximum applied load were carefully chosen based on some prior iteration tests and other references [5, 26] in order to satisfy the requirements for h_m, D, d, l and N in applying statistical nanoindentation technique to properly identify the microstructural phases and their properties. The requirements are as follows [19]:

$$D > 10h_m; h_m \gg d; l \gg D(N)^{-1/2} \tag{10}$$

where D is characteristic size of the phases; d is the largest heterogeneity of material; and l is the spacing between indenting points. D can be estimated to be 1–3 μm [20, 27], 1–50 μm, 50–300 μm, 5–50 μm for a well hydrated cement paste, silica powder, silica sand, and residual cement clinker (Table 1), respectively. On the other hand, the prime candidate for d can be the size of CSH sheet (≤ 2 nm) or the size of the single colloidal gel particles of 5 nm or crystal size of each phase, which is expected to be much smaller than h_m [5, 20, 27]. After the tests, the microstructure of the UHPC was captured using optical microscopy to examine the portions and the sizes of the microstructure phases in UHPC.

4. Results and discussion

4.1. Images of microstructure and nanoindentation response

Fig. 4 displays the optical microscopy images showing the microstructure of UHPC. As can be seen in this figure at the scale of 200 μm, the silica sand is clearly observed within the cement paste, whereas residual cement clinker and silica powder with various sizes of about 5–50 μm and 1–50 μm,

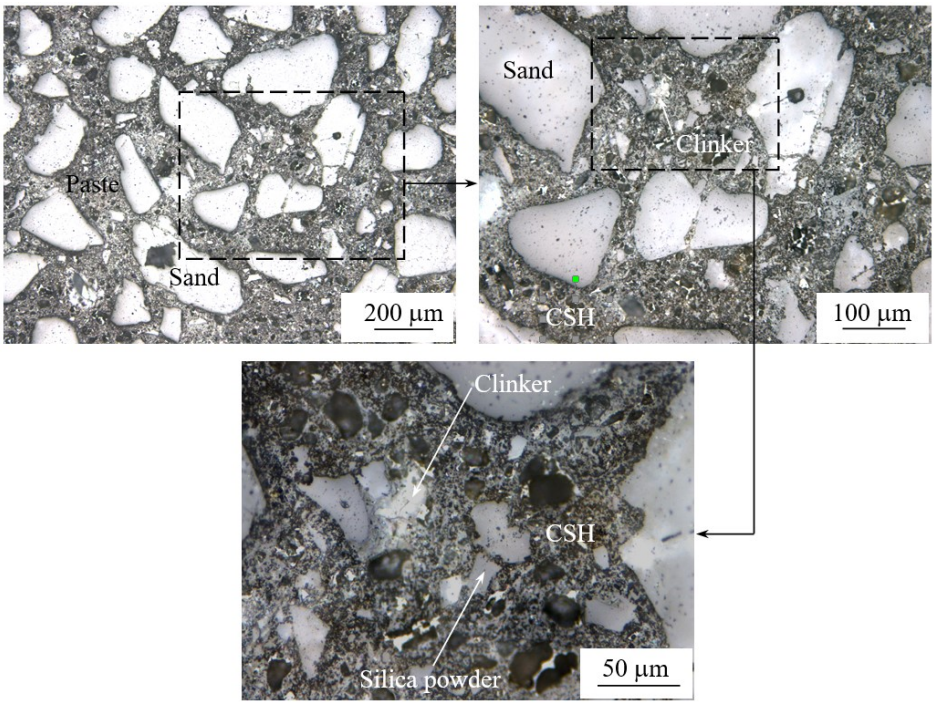

Figure 4. Optical microscopy images of UHPC microstructure

respectively, are visible in the cement paste at smaller scale. Fig. 5 presents the representative nanoindentaion curves measured in the phases, which are identified from the deconvolution analysis. It is noted that prior to the extraction of properties from $P - h$ curves for deconvolution analysis, all the curves were examined to ensure the validity of each curve. The irregular curves (curve with a "jump" in Fig. 5), which may be resulted from either severe fracture and damage during loading or improper contact detection when nanoindentation tests got undertaken on cracking [24], were easily detectable from visual inspection. Less than 5% irregular curves (26 curves) were detected and eliminated from the analysis, providing that with the maximum applied load of 2 mN, the maximum depth h_m measured from the phases varies from 50 to 220 μm.

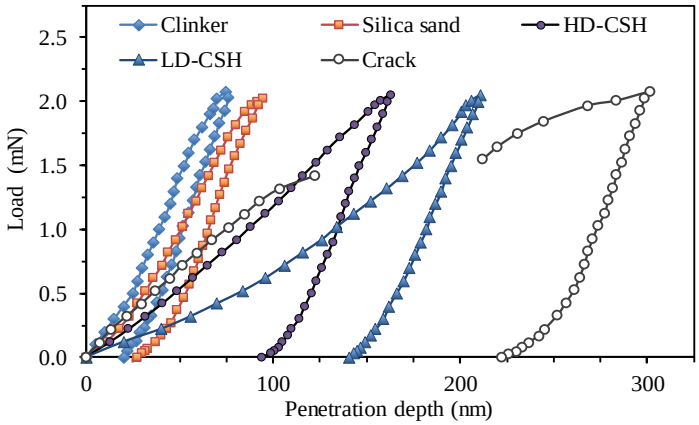

Figure 5. Representative nanoindentation $P - h$ curves

The observation from images of microstructure and representative $P - h$ curves measured from the phases in UHPC indicate that the separability scale conditions in Eq. (10) are satisfied and the properties extracted from $P - h$ curves can be used for deconvolution analysis.

4.2. Statistical deconvolution analysis results

The rest of nanoindentation curves after eliminating the irregular ones were used for the extraction of mechanical properties (M and H). The obtained M and H data from all tests were then utilized for the determination of the mechanically identifiable phases in UHPC by applying the statistical deconvolution analysis. For the statistical deconvolution analysis, the identifiable phases number n was searched to construct the best-estimated PDF that could accurately represent the experimental PDF of material properties. Based on the optical microstructure observations and the reported results on cement pastes and UHPC [5, 20, 26], the assumption that the UHPC microstructure consists of, at least, the following $n = 6$ phases is reasonable: (1) Porosity which includes the air voids resulted from the improper vibration and/or high fresh UHPC and capillary porosity with pore size less than 10 μm [5]; (2-3) Calcium Silicate Hydrates (CSH) which is characterized into at least two forms, LD CSH and HD CSH with different packing density, morphological arrangement, and mechanical properties [5, 19, 20, 26]; (4) Silica powder with the particle size in the range of from 1 to 50 μm; (5) Silica sand with the particle size in the range of from 50 to 300 μm, which is not reactive and dimensionally the largest granular material; (6) Residual cement clinker which always present in cement based materials with a w/c ratio < 0.42 and, as the hydration proceeds, the smallest particles dissolve first, and the large ones gradually start decreasing in size [5, 28, 29].

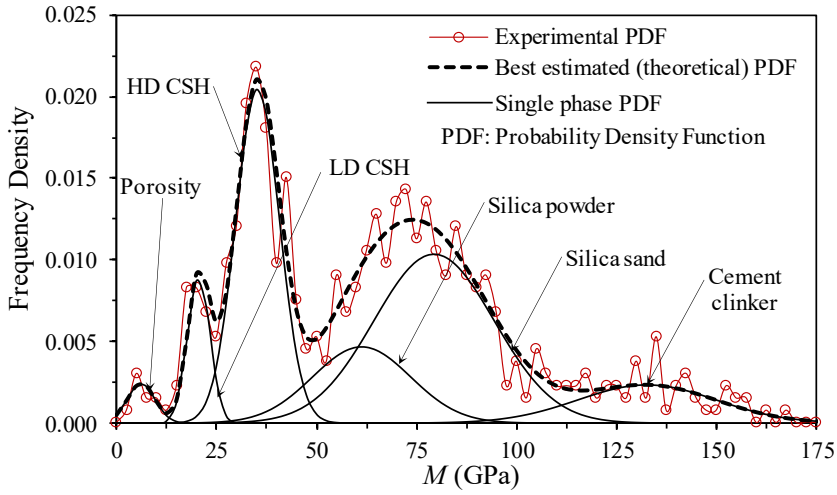

Figure 6. Deconvolution analysis results of M data

By minimizing Eq. (5) for the number of phases $n = 6$, the volume fraction and mechanical properties (M and H) of each mechanically distinguishable phase are obtained from the deconvolution analyses. Fig. 6 displays the experimental PDF (normalized histogram), the best-estimated (theoretical) probability distribution function (PDF), and each microstructure constituent determined from M spectrum. Those kinds of results determined from H spectrum are shown in Fig. 7. It is noted that the constrained condition in Eq. (9) was released for the case of silica powder and silica sand due to the fact that they are mainly made from the similar chemical compositions. However, they were divided into two separate phases considering their difference in particle size. The results of the deconvolution analysis process with regard to volume fraction, the mean and standard deviation of M and H of each constituent phase are summarized in Table 2, together with the reference values that reported in the literature.

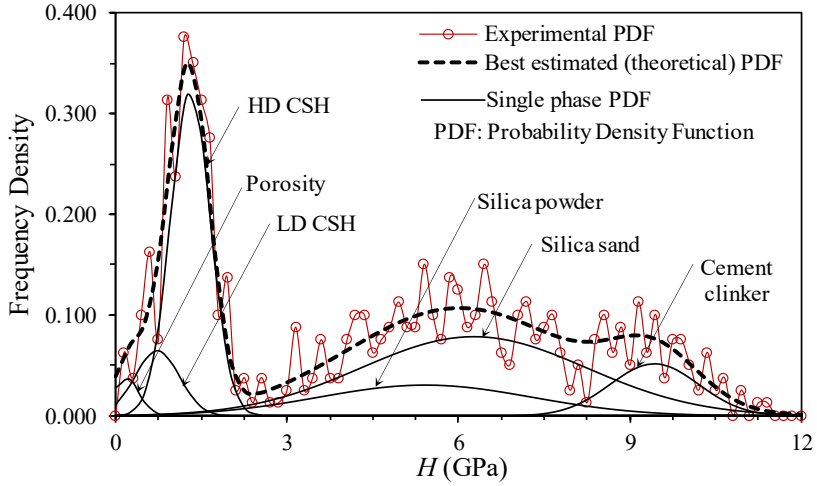

Figure 7. Deconvolution analysis results of H data

Table 2. Deconvolution analysis results with reference values reported in literature

Constituent phase	Obtained values			Reference values (Ref. in squared brackets)	
	Volume fraction	Modulus	Hardness	Modulus	Hardness
	f (%)	M (GPa)	H (GPa)	M (GPa)	H (GPa)
Micro porosity	2.1	6.21 ± 3.46	0.18 ± 0.22	7.0 ± 2.3 [5] 9.1 ± 2.3 [26]	0.19 ± 0.30 [5] 0.16 ± 0.07 [26]
LD-CSH	6.3	20.62 ± 2.83	0.73 ± 0.39	19.7 ± 2.5 [5] 19.1 ± 5.0 [27] 21.7 ± 2.2 [20] 20.2 ± 2.0 [29] 18.8 ± 4.0 [26] 23.7 ± 0.8 [30]	0.55 ± 0.03 [5] 0.80 ± 0.20 [29] 0.66 ± 0.30 [23] 0.47 ± 0.17 [26] 0.93 ± 0.11 [30]
HD-CSH	28.1	35.30 ± 5.48	1.31 ± 0.34	34.2 ± 5.0 [5] 29.4 ± 2.4 [20] 31.0 ± 4.0 [29] 32.3 ± 3.0 [23] 32.3 ± 2.6 [30]	1.36 ± 0.35 [5] 0.90 ± 0.30 [29] 1.29 ± 0.10 [23] 1.22 ± 0.07 [30]
Silica powder	14.3	61.28 ± 12.20	5.42 ± 1.87	58.5 ± 19.4 [5]	5.14 ± 3.08 [5]
Silica sand	39.1	79.41 ± 14.98	6.27 ± 1.93	76.3 ± 15.1 [5] 73.0 ± 1.6 [29]	5.14 ± 3.08 [5] 10.0 ± 0.3 [29]
Cement clinker	10.1	132.7 ± 17.29	9.43 ± 1.77	141.1 ± 34.8 [5] 125–145 ± 25 [28, 29] 126.8 ± 8.1 [30]	9.12 ± 0.9 [5] 8.0–10.8 ± 3 [28, 29] 6.7 ± 1.2 [30]

It can be seen from Table 2 that the volume fractions of the phases are reasonable and consistent with the composition as well as the observations of microstructure of UHPC shown in Fig. 4. The extracted mechanical properties including M and H are in the range of the reference values, and are in good agreement with the reported ones obtained from quite similar type of UHPC [5]. Indeed, the first peak with a mean modulus and hardness values of 6.21 GPa and 0.18 GPa of the best estimated *PDF* in Figs. 6 and 7, respectively, relates to the weakening effect of the micro porosity on the CSH matrix and can be considered as an indirect measure of the capillary porosity [5, 26, 27]. The mean values of modulus and hardness of the two next phases, i.e. LD-CSH and HD CSH, agree well with the corresponding values obtained from different cement pastes [20, 26, 27, 31]. Notably, the hardness of HD CSH agree well with corresponding one obtained from silimar UHPC [5], but is slightly enhanced with respect to the values reported for cement paste samples [29]. A remarkable result is that 81.7% percent of the total volume of the CSH matrix is HD CSH. This percentage is certainly much higher than 30%, which value is found for materials with a water to cement ratio $w/c = 0.5$ [20, 26]. Besides, the volume fractions of the two silica phases including powder and sand are consistent with the compostion of these particles in the UHPC compounds, where the latter is not reactive.

The mean values of both modulus and hardness of these phases are also in good agreement with the ones found in literature [5, 29]. Finally, highest peaks of both best estimated *PDF* curves are attributed to the residual cement clinker, which is characterized by a very high modulus and hardness of 132.7 ± 17.29 GPa and 9.43 ± 1.77 GPa with a volume content of about 10.1%. These extracted values are in line with the theoretical observation from the hydration reactions [28, 29]. The high standard deviation of the extracted modulus value of cement clinker may depend on the several clinker compounds (such as calcium silicate, calcium aluminate and calcium aluminoferite) which are not individually discernable by the present technique [5]. The mean hardness value of the cement clinker of 9.43 GPa is in good agreement with previous results on pure clinker phases [28, 29], while the high standard deviation has been normally obtained in heterogeneous cement pastes [26, 29]. Considering the experimental measurements' errors arising from material variability (chemical, casting, polishing...) and instrumented calibration, the obtained results in this study are acceptance and reliable.

5. Conclusions

In this study, the combined nanoindentation and statistical analysis were applied into a developed UHPC material to broaden the understanding of the microstructure phases and their mechanical properties. The following conclusions can be withdrawn:

- The modulus and hardness data obtained from a total of 550 grid nanoindentation tests can be used in the accurate and reliable identification of the microstructure phases and their properties in UHPC by applying statistical deconvolution analysis.

- For the present UHPC, the microstructure can be characterized into 6 phases with distinguishable mechanical properties, including micro porosity, LD and HD CSH, silica powder and sand, and residual cement clinker. The modulus and hardness values of these phases are obtained to be in the range of various reported ones for cement based materials and UHPC.

- The CSH matrix of UHPC is mainly composed of HD CSH, which is featured by intrinsic higher modulus and hardness values than LD CSH that dominates cement based materials with normal w/c ratio.

Acknowledgement

This research is supported by a grant (CT.2019.03.05) from Science and Technology Program funded by Ministry of Education and Training of Vietnam.

References

[1] Federal Highway Administration (2006). *Material property characterization of ultra-high performance concrete*. Publication No. FHWAHRT-06-103.

[2] Rebentrost, M., Wight, G., Fehling, E. (2008). Experience and applications of ultra-high performance concrete in Asia. In *2nd International Symposium on Ultra High Performance Concrete*, volume 10, 19–30.

[3] Shi, C., Wu, Z., Xiao, J., Wang, D., Huang, Z., Fang, Z. (2015). A review on ultra high performance concrete: Part I. Raw materials and mixture design. *Construction and Building Materials*, 101:741–751.

[4] Hoan, P. T., Thuong, N. T. (2019). Shear resistance of ultra-high-performance concrete reinforced with hybrid steel fiber subjected to impact loading. *Journal of Science and Technology in Civil Engineering (STCE) - NUCE*, 13(1):12–20.

[5] Sorelli, L., Constantinides, G., Ulm, F.-J., Toutlemonde, F. (2008). The nano-mechanical signature of Ultra High Performance Concrete by statistical nanoindentation techniques. *Cement and Concrete Research*, 38(12):1447–1456.

[6] Gautham, S., Sasmal, S. (2019). Recent Advances in Evaluation of intrinsic mechanical properties of cementitious composites using nanoindentation technique. *Construction and Building Materials*, 223: 883–897.

[7] Kim, J. J., Rahman, M. K., Taha, M. M. R. (2012). Examining microstructural composition of hardened cement paste cured under high temperature and pressure using nanoindentation and 29Si MAS NMR. *Applied Nanoscience*, 2(4):445–456.

[8] Hoan, P. T., Vinh, N. N., Tung, N. T. T. (2019). Indentation for investigation of strain rate effect on mechanical properties in structural steel weld zone. *Journal of Science and Technology in Civil Engineering (STCE) - NUCE*, 13(3):104–112.

[9] Pham, T.-H., Nguyen, N.-V. (2021). Mechanical properties of constituent phases in structural steels and heat-affected zones investigated by statistical nanoindentation analysis. *Construction and Building Materials*, 268:121211.

[10] Ulm, F.-J., Vandamme, M., Bobko, C., Ortega, J. A., Tai, K., Ortiz, C. (2007). Statistical Indentation Techniques for Hydrated Nanocomposites: Concrete, Bone, and Shale. *Journal of the American Ceramic Society*, 90(9):2677–2692.

[11] Nguyen, N.-V., Pham, T.-H., Kim, S.-E. (2019). Strain rate sensitivity behavior of a structural steel during low-cycle fatigue investigated using indentation. *Materials Science and Engineering: A*, 744:490–499.

[12] Luo, Z., Li, W., Gan, Y., Mendu, K., Shah, S. P. (2020). Applying grid nanoindentation and maximum likelihood estimation for N-A-S-H gel in geopolymer paste: Investigation and discussion. *Cement and Concrete Research*, 135:106112.

[13] Oyen, M. (2010). *Handbook of Nanoindentation*. Pan Stanford Publishing.

[14] Oliver, W. C., Pharr, G. M. (1992). An improved technique for determining hardness and elastic modulus using load and displacement sensing indentation experiments. *Journal of Materials Research*, 7(6):1564–1583.

[15] Vinh, N. N., Anh, V. Q., Thang, H. T. (2020). Characterization of strain amplitude-dependent behavior of hardness and indentation size effect of SS400 structural steel. *Journal of Science and Technology in Civil Engineering (STCE) - NUCE*, 14(3):15–25.

[16] Nguyen, N.-V., Kim, S.-E. (2020). Experimental study to investigate microstructure and continuous strain rate sensitivity of structural steel weld zone using nanoindentation. *International Journal of Mechanical Sciences*, 174:105482.

[17] Nguyen, N.-V., Pham, T.-H., Kim, S.-E. (2019). Strain rate-dependent behaviors of mechanical properties of structural steel investigated using indentation and finite element analysis. *Mechanics of Materials*, 137: 103089.

[18] Constantinides, G., Chandran, K. S. R., Ulm, F.-J., Vliet, K. J. V. (2006). Grid indentation analysis of composite microstructure and mechanics: Principles and validation. *Materials Science and Engineering: A*, 430(1-2):189–202.

[19] Constantinides, G., Ulm, F.-J. (2007). The nanogranular nature of C–S–H. *Journal of the Mechanics and Physics of Solids*, 55(1):64–90.

[20] Constantinides, G., Ulm, F.-J. (2004). The effect of two types of C-S-H on the elasticity of cement-based materials: Results from nanoindentation and micromechanical modeling. *Cement and Concrete Research*, 34(1):67–80.

[21] Meister, A. (2009). *Deconvolution Problems in Nonparameteric Statistics*. Lecture Notes in Statistics.

[22] ASTM C 1437 (2001). *Standard Test Method for Flow of Hydraulic Cement Mortar*. ASTM International.

[23] ASTM Standard E3-01 (2007). *Standard Guide for Preparation of metallographic specimens*. ASTM International.

[24] Pathak, S., Stojakovic, D., Doherty, R., Kalidindi, S. R. (2009). Importance of surface preparation on the nano-indentation stress-strain curves measured in metals. *Journal of Materials Research*, 24(3):1142–1155.

[25] ASTM E2546-07 (2007). *Standard Practice for Instrumented Indentation Testing*. ASTM International, West Conshohocken, PA.

[26] G. Constantinides, F.-J. U. (2006). *The elastic properties of calcium leached cement pastes and mortars: a multi-scale investigation*.

[27] DeJong, M. J., Ulm, F.-J. (2007). The nanogranular behavior of C-S-H at elevated temperatures (up to 700 °C). *Cement and Concrete Research*, 37(1):1–12.

[28] Velez, K., Maximilien, S., Damidot, D., Fantozzi, G., Sorrentino, F. (2001). Determination by nanoindentation of elastic modulus and hardness of pure constituents of Portland cement clinker. *Cement and Concrete Research*, 31(4):555–561.

[29] Acker, P. (2001). *Micromechanical analysis of creep and shrinkage mechanisms*. Creep, Shr, Elsevier, Oxford, UK.

[30] Mondal, P., Shah, S. P., Marks, L. (2007). A reliable technique to determine the local mechanical properties at the nanoscale for cementitious materials. *Cement and Concrete Research*, 37(10):1440–1444.

[31] Miller, M., Bobko, C., Vandamme, M., Ulm, F.-J. (2008). Surface roughness criteria for cement paste nanoindentation. *Cement and Concrete Research*, 38(4):467–476.